

PLANETARY TRANSIT CANDIDATES IN THE CSTAR FIELD: ANALYSIS OF THE 2008 DATA

SONGHU WANG¹, HUI ZHANG¹, JI-LIN ZHOU¹, XU ZHOU^{2,3}, MING YANG¹, LIFAN WANG⁴, D. BAYLISS⁵, G. ZHOU⁵, M. C. B. ASHLEY⁶, ZHOU FAN^{2,3}, LONG-LONG FENG⁴, XUEFEI GONG⁷, J. S. LAWRENCE^{6,8}, HUIGEN LIU¹, QIANG LIU², D. M. LUONG-VAN⁶, JUN MA^{2,3}, ZEYANG MENG¹, J. W. V. STOREY⁶, R. A. WITTENMYER⁶, ZHENYU WU^{2,3}, JUN YAN², HUIGEN YANG⁹, JI YANG⁴, JIAYI YANG¹, XIANGYAN YUAN⁷, TIANMENG ZHANG^{2,3}, ZHENXI ZHU⁴, AND HU ZOU^{2,3}

¹ School of Astronomy and Space Science and Key Laboratory of Modern Astronomy and Astrophysics in Ministry of Education, Nanjing University, Nanjing 210093, China; zhoujl@nju.edu.cn

² National Astronomical Observatories, Chinese Academy of Sciences, Beijing 100012, China; zhouxu@bao.ac.cn

³ Key Laboratory of Optical Astronomy, National Astronomical Observatories, Chinese Academy of Sciences, Beijing 100012, China

⁴ Purple Mountain Observatory, Chinese Academy of Sciences, Nanjing 210008, China

⁵ Research School of Astronomy and Astrophysics, Australian National University, Canberra, ACT 2611, Australia

⁶ School of Physics, University of New South Wales, NSW 2052, Australia

⁷ Nanjing Institute of Astronomical Optics and Technology, Nanjing 210042, China

⁸ Australian Astronomical Observatory, NSW 1710, Australia

⁹ Polar Research Institute of China, Pudong, Shanghai 200136, China

Received 2013 November 2; accepted 2014 February 20; published 2014 March 27

ABSTRACT

The Chinese Small Telescope ARray (CSTAR) is a group of four identical, fully automated, static 14.5 cm telescopes. CSTAR is located at Dome A, Antarctica and covers 20 deg² of sky around the South Celestial Pole. The installation is designed to provide high-cadence photometry for the purpose of monitoring the quality of the astronomical observing conditions at Dome A and detecting transiting exoplanets. CSTAR has been operational since 2008, and has taken a rich and high-precision photometric data set of 10,690 stars. In the first observing season, we obtained 291,911 qualified science frames with 20 s integrations in the *i* band. Photometric precision reaches ~4 mmag at 20 s cadence at *i* = 7.5 and is ~20 mmag at *i* = 12. Using robust detection methods, 10 promising exoplanet candidates were found. Four of these were found to be giants using spectroscopic follow-up. All of these transit candidates are presented here along with the discussion of their detailed properties as well as the follow-up observations.

Key words: methods: data analysis – planetary systems – surveys – techniques: photometric

1. INTRODUCTION

The detection and study of exoplanets is one of the most exciting and fastest growing fields in astrophysics. At the present time, several different detection methods have yielded success. Two of the most productive methods have been the radial velocity (RV) method and the transit method. Although among the confirmed exoplanets, the RV method has been more productive, the transit method also has its advantages. The spectroscopic RV method measures the doppler velocity signatures of individual stars at multiple epochs, which is a very time-consuming procedure. The photometric transit method can yield the light curves of thousands of stars simultaneously. More importantly, the photometric transit method provides information on planetary radius and the inclination of the planetary orbit relative to the line of sight, which is not possible from RV detections. In addition, a wide array of studies are possible for transiting exoplanets, which cannot be done with non-transiting systems, e.g., the study of planetary atmospheres (Sing et al. 2009), temperature, surface brightness (Snellen & Covino 2007; Snellen et al. 2010), and the misalignment between the planetary orbit and the stellar spin (Winn et al. 2005).

Ideally, the search for transit exoplanet requires high-quality, wide-field, long-baseline continuous time-series photometry. This kind of monitoring can be achieved effectively by ambitious space-based programs such as *CoRoT* (Baglin et al. 2006) and *Kepler* (Borucki et al. 2010) or complicated longitude-distributed network programs such as HATNet (Bakos et al. 2004) and HATSouth (Bakos et al. 2013). However, the circumpolar locations offer a potentially comparable alternative.

The circumpolar locations provide favorable conditions for a wide and diverse range of astronomical observations, including photometric transiting detections. Thanks to the extremely cold, calm atmosphere and thin turbulent surface boundary layer, as well as the absence of light and air pollution, we can obtain high-quality photometric images in circumpolar locations (Burton 2010; Steinbring et al. 2010, 2012, 2013). Furthermore, the long polar nights offer an opportunity to obtain continuous photometric monitoring. As shown by a series of previous thorough and meticulous studies (cf. Pont & Bouchy 2005; Crouzet et al. 2010; Daban et al. 2010; Law et al. 2013), it greatly increases the detectability of transiting exoplanets, particularly those with periods in excess of a few days. Additionally, decreased high-altitude turbulence will result in reduced scintillation noise that will lead to superior photometric precision (Kenyon et al. 2006). The significant photometric advantages of the polar regions have been proven and utilized by the observing facilities at different polar sites such as two AWCam (Law et al. 2013) at the Canadian High Arctic; SPOT (Taylor et al. 1988) at the South Pole; and the small-IRAIT (Tosti et al. 2006), ASTEP-South (Crouzet et al. 2010), and ASTEP-400 (Daban et al. 2010) at Dome C.

Dome A, located in the deep interior of Antarctica, with a surface elevation of 4093 m, is the highest astronomical site on the continent and is also one of the coldest places on Earth. In a study that considered the weather, the boundary layer, air glow, aurorae, precipitable water vapor, surface temperature, thermal sky emission, and the free atmosphere, Saunders et al. (2009) concluded that Dome A might be the best astronomical site on Earth.

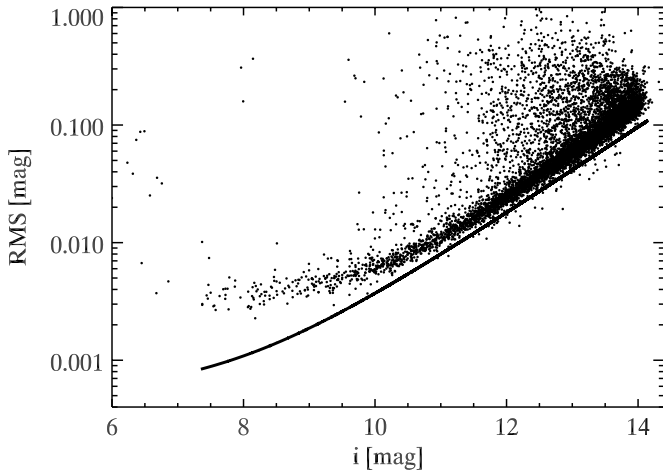


Figure 1. Distribution of rms values at 20 s cadence as a function of CSTAR i magnitude. Each point represents a light curve. Photometric precision of resulting CSTAR light curve is typically ~ 20 mmag at $i = 12$, with ~ 4 mmag achieved at $i = 7.5$. We over-plotted the theoretic rms as a function of magnitude, taking into account the photon and sky background noise as well as the scintillation noise.

In order to take advantage of these remarkable observing conditions at Dome A, the Chinese Small Telescope ARray (CSTAR) was established there in 2008 January. CSTAR undertook both site testing and science research tasks. In 2008, 291,911 qualified i -band photometric images were acquired. Based on these data, the first version of a photometric catalog was released by Zhou et al. (2010a); this catalog has been updated three times (Wang et al. 2012, 2014; Meng et al. 2013) to correct for various systematic errors. The resulting CSTAR photometric precision typically reaches ~ 4 mmag at 20 s cadence at $i = 7.5$, and is ~ 20 mmag at $i = 12$ (see Figure 1), which is sufficient for the detection of giant transiting exoplanets around F, G, K dwarf stars.

In this paper, we present 10 exoplanet candidates from 10,690 high-precision light curves selected from the CSTAR data of 2008 (Wang et al. 2014). Of these candidates, four were found to be giants using spectroscopic follow-up. Since this is the first effort to find exoplanets from these data, we describe the CSTAR instrument, observations, previous data reductions, and the methods used for the transit searching in detail as well as the procedures used to eliminate the false positives.

The layout of the paper is as follows. A brief description of the CSTAR instrument, observations, and previous data reduction as well as the photometric precision of the light curves is presented in Section 2. In Section 3, we detail the techniques we used for transit detection and the robust procedures of data validation. The spectroscopic and RV follow-up are briefly described in Section 4. We report the exoplanet candidates along with the detailed properties for each system in Section 5. Lastly, the work is summarized and prospects for future work are discussed in Section 6.

2. INSTRUMENT, OBSERVATIONS, AND PREVIOUS DATA PROCESSING

2.1. Instrument

CSTAR, as a part of PLATEau Observatory (Lawrence et al. 2009; Yang et al. 2009), is the first photometric instrument to enter operation at Dome A. Full details of the CSTAR instrument can be found in Yuan et al. (2008) and Zhou et al. (2010b). Here we summarize the features relevant to this work. The CSTAR

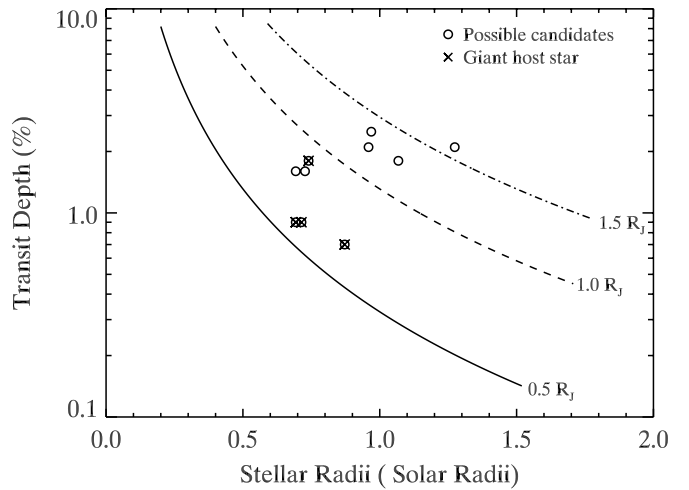


Figure 2. Transit depth plotted as a function of stellar radius. Over-plotted are curves showing the expected transit depth for planets with radii of 0.5, 1.0, and 1.5 R_J assuming centrally crossing transit ($i = 90^\circ$).

facility consists of four static, co-aligned Schmidt–Cassegrain telescopes on a fixed mount with the same $4.5^\circ \times 4.5^\circ$ field of view (FOV) around the South Celestial Pole, each telescope housing a different filter in Sloan Digital Sky Survey (SDSS) bands: r , g , i and $open$. Each telescope gives a 145 mm entrance pupil diameter (effective aperture of 100 mm) and is coupled to a $1K \times 1K$ Andor DV 435 frame transfer CCD array which yields a plate-scale of $15 \text{ arcsec pixel}^{-1}$.

2.2. Observations

CSTAR was successfully shipped to and deployed at Dome A in 2008 January and operated for the subsequent 4 yr. This work is based on the data obtained in 2008. In the 2008 observing season (2008 March 4 to August 8), intermittent problems with the CSTAR computers and hard disks (Yang et al. 2009) prevented us from obtaining useful data in the g , r , and $open$ bands. Fortunately the i band data were not affected, and observations were carried out for 1728 hr (291,911 qualified frames with 20 s exposure times) during the Antarctic polar nights with only a few short interruptions due to cloudy weather (Zou et al. 2010) or temporary instrument problems (Yang et al. 2009). These observations provide well-sampled light curves with a baseline of more than one hundred days. Additional details of the CSTAR observations in 2008 are presented in Zhou et al. (2010a).

2.3. Previous Data Reductions

Reduction of the CSTAR data aim to produce millimagnitude photometric precision for the bright stars. A custom reduction pipeline was developed which is able to achieve this goal and is described in more detail in Zhou et al. (2010a) and Wang et al. (2012, 2014) as well as Meng et al. (2013). Here we will only briefly review the main factors to be considered when reducing the wide-field data from CSTAR.

After preliminary reductions, aperture photometry was performed on the sources that were detected in all calibrated images. Using the 48 brightest local calibrators, the instrumental magnitudes were calibrated to the i magnitudes of the stars in the USNO-B 1.0 catalog (Monet et al. 2003), which were derived from the UNSO-B 1.0 mag according to the transformation between USNO-B 1.0 mag and SDSS i magnitude given

Table 1
Summary of CSTAR Exoplanet Transit Candidates

CSTAR ID	Epoch	i	Period	Duration	Depth	R_*	R_p	$B-V$	$J-K$	T_{eff}	$\log(g)$	S_p	$\Delta x^2 / \Delta x^2_{-}$	S/N_{ellip}	S_r	η	P_{δ}	P_t
CSTAR J+	(2454500.0+)	(mag)	(days)	(hr)	(mag)	(R_{\odot})	(R_{Jup})	(mag)	(mag)	(K)								
183056.78-884317.0	53.69665	9.84	9.924	10.004	0.021	1.214	1.531	0.48	0.31	F5	4.23	5.87	22.32	2.03	0.42	0.38
001238.65-871811.0	48.80221	10.59	5.371	2.269	0.021	0.959	1.356	0.69	0.43	5900	4.9	G5	3.53	0.28	8.78	0.65	0.66	0.74
014026.01-873057.1	46.69858	10.26	4.164	1.847	0.009	0.714	0.519	1.54	0.67	4800	0.6	Giant	1.48	0.26	10.37	0.71	0.15	0.44
021535.71-871122.5	46.50898	10.69	1.438	1.360	0.018	0.740	0.862	1.65	0.80	4600	3.3	Giant	2.69	0.45	12.10	0.71	0.48	0.23
022810.02-871521.3	50.90359	10.62	2.586	2.048	0.021	1.274	1.547	0.44	0.36	6100	3.5	F5	2.63	0.65	7.11	0.61	0.64	0.11
075108.62-871131.3	47.59870	10.41	2.630	2.298	0.016	0.693	0.742	1.24	0.95	4800	4.5	K7	1.52	0.75	8.60	1.02	0.17	0.42
110005.67-871200.4	47.11239	10.84	3.228	1.633	0.025	0.969	1.335	0.68	0.33	6300	3.9	G5	2.02	1.19	10.60	0.55	0.07	0.62
113310.22-865758.3	47.14206	9.97	1.652	2.045	0.016	0.727	0.794	1.06	0.60	4900	5.0	K4	1.63	1.72	6.96	1.03	0.45	0.40
132821.71-870903.3	46.53672	10.41	4.273	1.797	0.018	1.068	1.255	0.59	0.41	6000	4.5	G0	1.62	2.17	7.05	0.53	0.01	0.20
203905.43-872328.2	47.21003	10.35	2.216	2.691	0.007	0.872	0.636	0.79	0.68	4800	1.5	Giant	1.64	0.53	7.68	1.15	0.22	0.91
231620.78-871626.8	46.99121	10.76	1.408	1.676	0.009	0.693	0.569	1.39	0.81	4300	2.4	Giant	2.86	0.36	6.68	0.94	0.02	0.82

by Monet et al. (2003). Finally, the first version of the CSTAR catalog, detailed in Zhou et al. (2010a), was released.

For transit searching, the photometric data were further refined by applying corrections for additional systematic errors, as briefly reviewed below.

Poor weather will lead to spatial variations in extinction across the large CSTAR FOV ($4^{\circ}5 \times 4^{\circ}5$). This spatially uneven extinction can be modeled and corrected by comparing each frame to a master (median) frame. More detailed procedures have been described in Wang et al. (2012).

The residual of the flat-field correction results in spatially dependent errors, which show up as daily variations when the stars are centered on the different pixels in different exposure frames during their diurnal motion around the south celestial pole on the static CSTAR optical system. This kind of diurnal effect can be effectively corrected by specific differential photometry: comparing the target object to a bright reference star in the nearby diurnal path. For more details, see Wang et al. (2014).

Since CSTAR is a static telescope and fixed to point at the South Celestial Pole, star images move clockwise on the CCD due to diurnal motion. Ghost images, located in the symmetrical position of the CCD, move counterclockwise. Because of this, ghost images move and contaminate the photometry of stars. The significant contamination arising from the ghost images, detailed in Meng et al. (2013), was also studied and corrected.

The resulting light curves typically achieve a photometric precision of ~ 4 mmag at 20 s cadence for the brightest non-saturated stars ($i = 7.5$), rising to ~ 20 mmag at $i = 12$. The distribution of rms values as a function of i magnitude is shown in Figure 1. Each of the points represents a 20 s sampled light curve with one-day observations. The abrupt upturn in variability at $i < 7.5$ signifies the onset of saturation, and our photometry is complete to a limiting magnitude of $i = 14$. For that reason, we use the i -band time-series data on the 10,690 point sources, restricted to $7.5 < i < 14$ in our study, to detect transit events.

3. TRANSIT DETECTION

3.1. Transit Searching Algorithm

To search for planetary transits in the light curves, the BLS algorithm (Kovács et al. 2002) is applied to the data. The search is limited within the 1.05–30.0 day period range, with 4500 period steps, 1500 phase bins, and a fractional transit length from $q_{\text{min}} = 0.01$ to $q_{\text{max}} = 0.1$. The BLS spectra of CSTAR light curves generally display an increasing background power toward lower frequencies. This is caused by slight long-term systematic trends of the light curves (Bakos et al. 2004). To remove this effect from the BLS spectra, a fourth-order polynomial is fitted and then subtracted from the spectra. For the most significant residual peaks which do not lie at a known alias, fit statistics and parameters of the box-fitting transit model are obtained and then used to provide a ranked list of the best candidates.

3.2. Candidate Selection Criteria

The systematic errors and true astrophysical variabilities, such as low-mass star, “blended stellar binaries,” and “grazing stellar binaries,” can mimic true transit signals and result in a high false-positive rate. For this reason, it is imperative to distinguish false-positive signals from true exoplanet candidates. This section describes the procedures of candidate inspection based on the techniques used in previous successful transit surveys such as WASP (Pollacco et al. 2006), HATNet (Bakos et al. 2004), HATSouth (Bakos et al. 2013), *CoRoT* (Baglin et al. 2006), Optical Gravitational Lensing Experiment (OGLE; Udalski et al. 2002), *Kepler* (Borucki et al. 2010), XO (McCullough et al. 2005), and the Trans-Atlantic Exoplanet Survey (Alonso et al. 2004).

3.2.1. Stage 1: Pre Filter

As described in Section 2.3, a total of 10,690 stars with sufficiently high precision were selected from the CSTAR data set

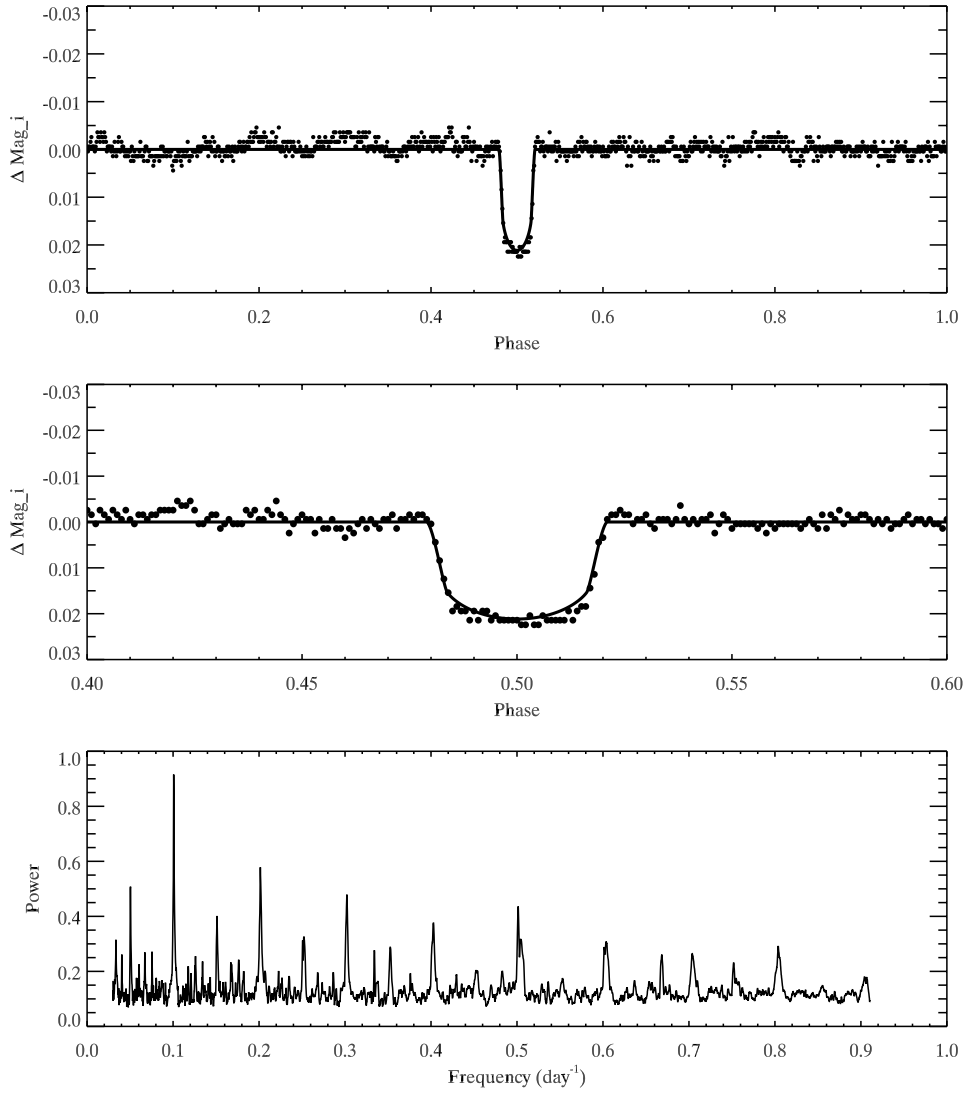


Figure 3. Full (top panel) and zoom-in (middle panel) binned phase-folded ($p = 9.924$ days) light curve (filled circles) along with the normalized and detrended BLS periodogram (bottom panel) of CSTAR J183056.78-884317.0 ($i = 9.84$). The solid line in the top and middle panels show the best-fit transit model (JKTEBOP). For clarity, the phased light curve was binned into 1000 bins. The binned light curve is shown for visualization only and was not used in our analysis.

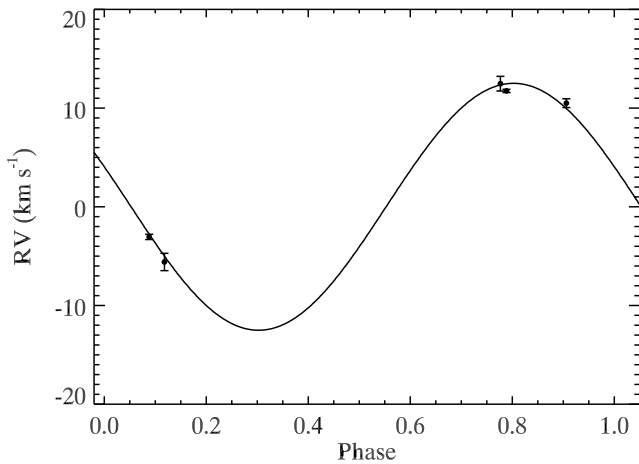


Figure 4. Radial velocity measurements (filled circles) for CSTAR J183056.78-884317.0 from the WiFeS and echelle instruments on ANU 2.3 m telescope, together with $e = 0$ fit model (solid curve). The semi-amplitude of the best fit $e = 0$ orbit gives $K = 12 \text{ km s}^{-1}$, indicating this is an eclipsing binaries system. This is consistent with our results derived from analysis of the transit duration and ellipsoidal variation.

for transit searching. They are processed by the detection algorithm, yielding an output of fit statistics and parameters of the box-fitting transit model. The large number of stars make visual inspection of every light curve infeasible, so we require that a number of conditions be satisfied before subjecting the candidates to visual inspection. To avoid missing any interesting candidates before visual inspection, the initial selection criteria are deliberately set relatively low. The thresholds for rejection are:

1. A photometric transit depth greater than 10%. The fractional change in brightness of transit depth is essentially determined by the square of the ratio of the planet radius to the host star radius. Giant transiting planets typically have depths on the order of 1%. We set a relatively loose depth criteria (10%) to avoid loss of interesting objects. Although a $R = 2 R_J$ planet will block out a quarter of the light of late-type stars (e.g., M0 V star), as Kane et al. (2008) pointed out, these kinds of detections from bright, wide-field surveys would be extremely rare.
2. Frequencies with empty phases. The incomplete phase coverage leads to aliasing and can often cause false-positive detection. We use a simple model to exclude frequencies

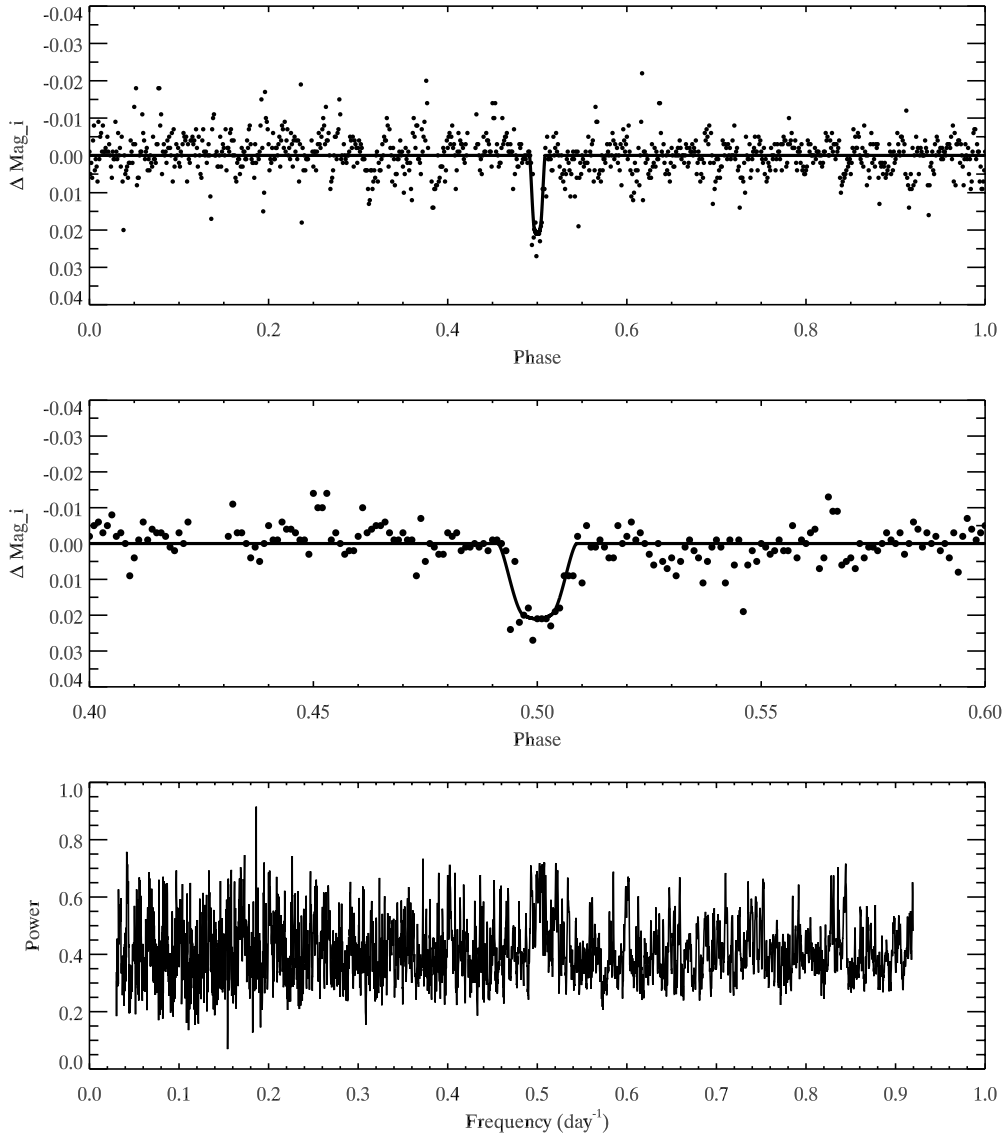


Figure 5. Same as Figure 3, but phase folded for $p = 5.371$ days for CSTAR J001238.65-871811.0 ($i = 10.59$).

with poor phase coverage. The folded light curve is split with the expected transit width. A frequency is considered systematic if the number of empty intervals is larger than two.

3. *A Period < 1.05 day or periods at a known alias.* The BLS algorithm, similar to other pattern matching methods, suffers from aliasing effects originating from nearly periodic sampling (Kovács et al. 2002). Therefore, it creates false frequency peaks at periods associated with one sidereal day and a uniform 20 s sampling interval. The BLS spectra clearly display such peaks, as well as some other commonly occurring frequencies associated with the remaining systematic errors. For that reason stars exhibiting these periodicities are excluded in order to minimize the number of aliases. We have also elected not to search for transits with periods less than 1.05 days, due to the large number of false frequency peaks in that region.

Even these relatively low selection criteria remove more than 85% of the initial detections. Only 1583 candidates pass and these are then visually inspected as set out in the next section.

3.2.2. Stage 2: Visual Inspection

Our visual inspection procedure is based upon that used for the successful WASP program as described in Clarkson et al. (2007), Lister et al. (2007) and Street et al. (2007).

During the visual inspection of the folded light curves in conjunction with the corresponding BLS spectra, surviving candidates are required to have the following:

1. *A plausible transit shape.* Since the transit depth has been limited in *stage 1*, transit shape becomes the first important aspect in this stage. A visible transit dip is a basic requirement for a candidate to be called a “transit candidate.”
2. *A flat out-of-transit light curve.* The light curve before and after transit should be flat. Candidates are removed if they show clear evidence of variability out of transit, including a secondary eclipse, ellipsoidal variation, as well as realistic variability of other forms.
3. *A smooth phase coverage.* Although candidates were systematically removed in *stage 1* if their frequencies were associated with gaps in the folded light curves, some with uneven distribution of data points in the folded light curves,

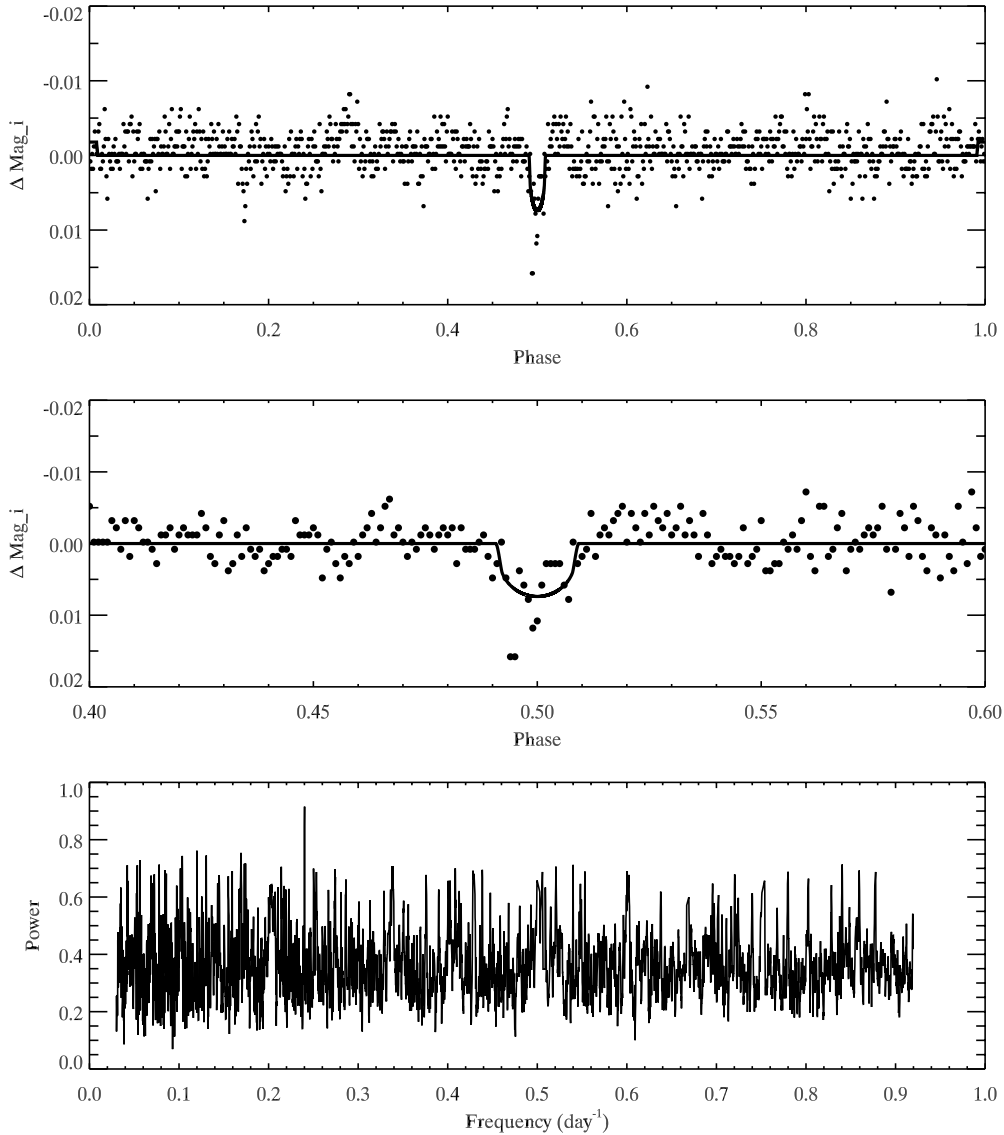


Figure 6. Same as Figure 3, but phase folded for $p = 4.164$ days for CSTAR J014026.01-873057.1 ($i = 10.26$).

which may not be effectively identified in *stage 1*, were deselected from further consideration by visual inspection.

This step is also used to discard light curves of poor quality.

4. *A credible measured period.* BLS spectra together with the folded light curves are inspected to confirm whether the clear period peaks are arising from secure transit signals or other variabilities.

As the visual inspection process is somewhat subjective, it was carried out independently by each of the two authors (Songhu Wang and Ming Yang). After a comparison of the analysis, this examination reduced the 1583 candidates to 208 transit-like candidates, which required further investigation.

3.2.3. Stage 3: Statistical Filter

The main purpose of this stage is to facilitate the further identification of the true planetary candidates from false-positive transit detections caused by systematic trends or true astrophysical variability. Candidates are passed forward if:

1. *The signal-to-red noise (S_r) ≥ 7.0 .* Contrary to the white noise (uncorrelated-noise) assumptions, the errors on ground-based millimagnitude photometry are usually

red (correlated) (Pont et al. 2006). In the CSTAR data, the uncertainty of the mean decreases more slowly than $n^{1/2}$, suggesting that red noise is present. This can mimic transit signal with a time-scale similar to the duration of the true close-in planetary transit. So, S_r , a simple and robust statistical parameter to assess the significance level of detected transit in the presence of red noise, is calculated for each light curve by

$$S_r = \frac{d\sqrt{N_{tr}}}{\sigma_r}, \quad (1)$$

where d is the best-fitting transit depth, N_{tr} is the number of transits observed, and σ_r is the uncertainty of transit depth binned on the expected transit duration in the presence of red noise. The simplest method of assessing the level of red noise (σ_r) present in the data is to compute a sliding average of the out-of-transit data over the n data points contained in a transit-length interval. This method is proposed by Pont et al. (2006) and has been successfully applied to the SuperWASP candidates (Christian et al. 2006; Clarkson et al. 2007; Kane et al. 2008; Lister et al. 2007; Street et al.

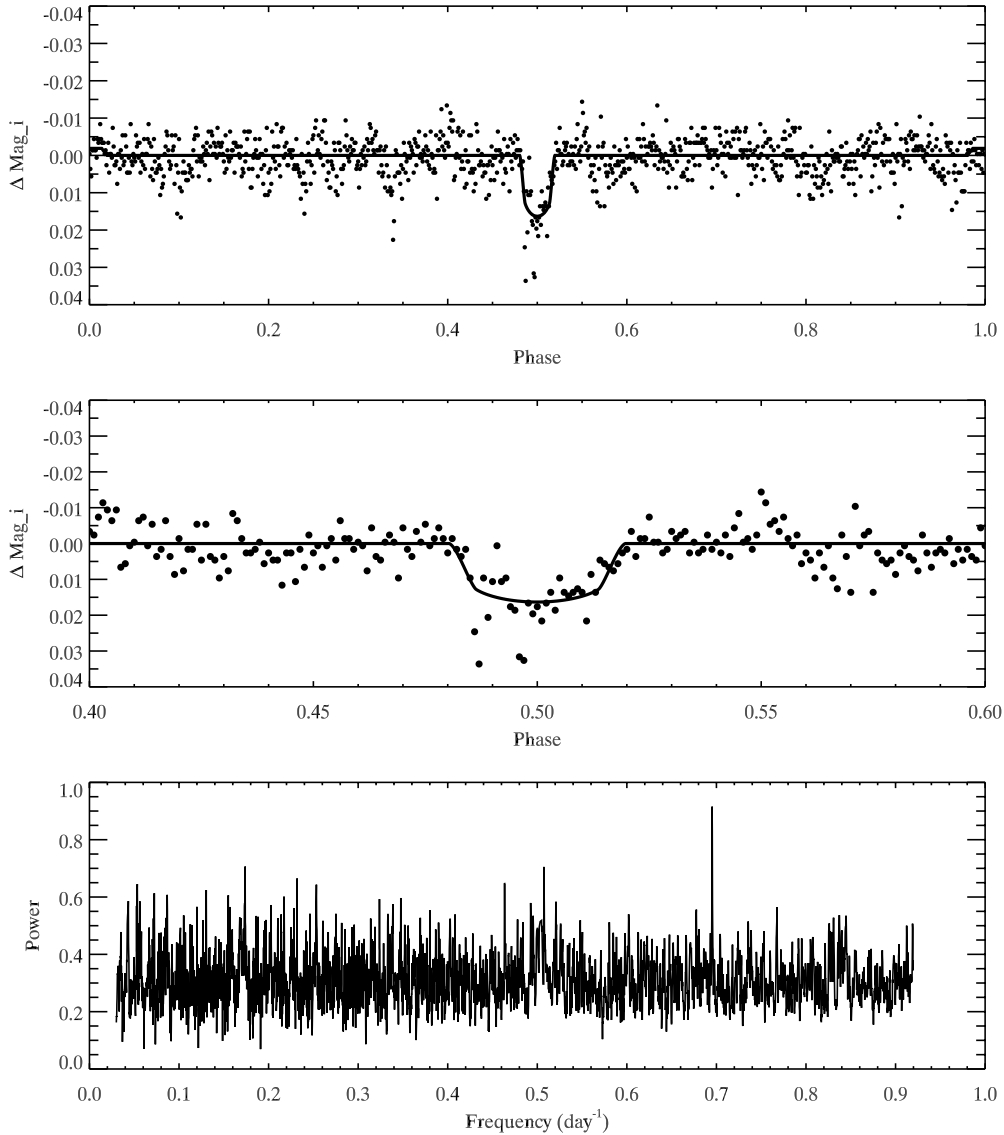


Figure 7. Same as Figure 3, but phase folded for $p = 1.438$ days for CSTAR J021535.71-871122.5 ($i = 10.69$).

- 2007). The typical level of σ_r in the CSTAR data is of 2.1 mmag. It is slightly lower when compared to 3 mmag for OGLE (Pont et al. 2006) and SuperWASP (Smith et al. 2006). For that reason, although there is no confirmed planetary transit and no simulation was performed for the S_r threshold in the CSTAR survey to attempt to detect more transiting planets, it is reasonable to set our S_r threshold to the lower boundary of the typical range (7–9) of that given by Pont et al. (2006) based on the detailed simulation with $S_r = 3$ mmag. This threshold is also consistent with that used for the SuperWASP candidates (Christian et al. 2006).
2. *The transit to antitransit ratio* ($\Delta\chi^2/\Delta\chi_-^2 \geq 1.5$). The systematic variations and the stellar intrinsic variables with timescales similar to the planetary transit can give rise to false-positive transit detections. A light curve with a genuine transit will result in only a strong transit (dimming) detection and not a strong antitransit (brightening) detection. On the contrary, one could expect that the strong correlated measurements caused by the systematics or the stellar intrinsic variables should produce both significant transit and

antitransit detections. Consequently, $\Delta\chi^2/\Delta\chi_-^2$, measuring the ratio of improvements of best-fit transit to the improvements of the best-fit antitransit, is calculated for each light curve. This provides an estimate to which a detection has the expected properties of a credible transit signal rather than the properties of the systematics or intrinsic stellar sinusoidal variability (Burke et al. 2006).

3. *The signal-to-noise of the ellipsoidal variation* ($S_{\text{ellip}} < 5.0$). Blended systems, gazing eclipsing binaries, and eclipsing systems with a planet-sized star (e.g., brown dwarf) are the most common astrophysical imposters that mimic a transiting planet signal. It can be very difficult to distinguish these systems from genuine transiting planets using the properties of the transit event itself (e.g., shape, depth, etc). Nevertheless, evidence of ellipsoidal variability, due to tidal distortions and gravity brightening, can be used to remove from the remaining candidates which have massive, and therefore not planetary, companions. The method proposed by Sirko & Paczyński (2003) was successfully applied to the OGLE (Udalski et al. 2002) and the WASP (Pollacco et al. 2006) candidates.

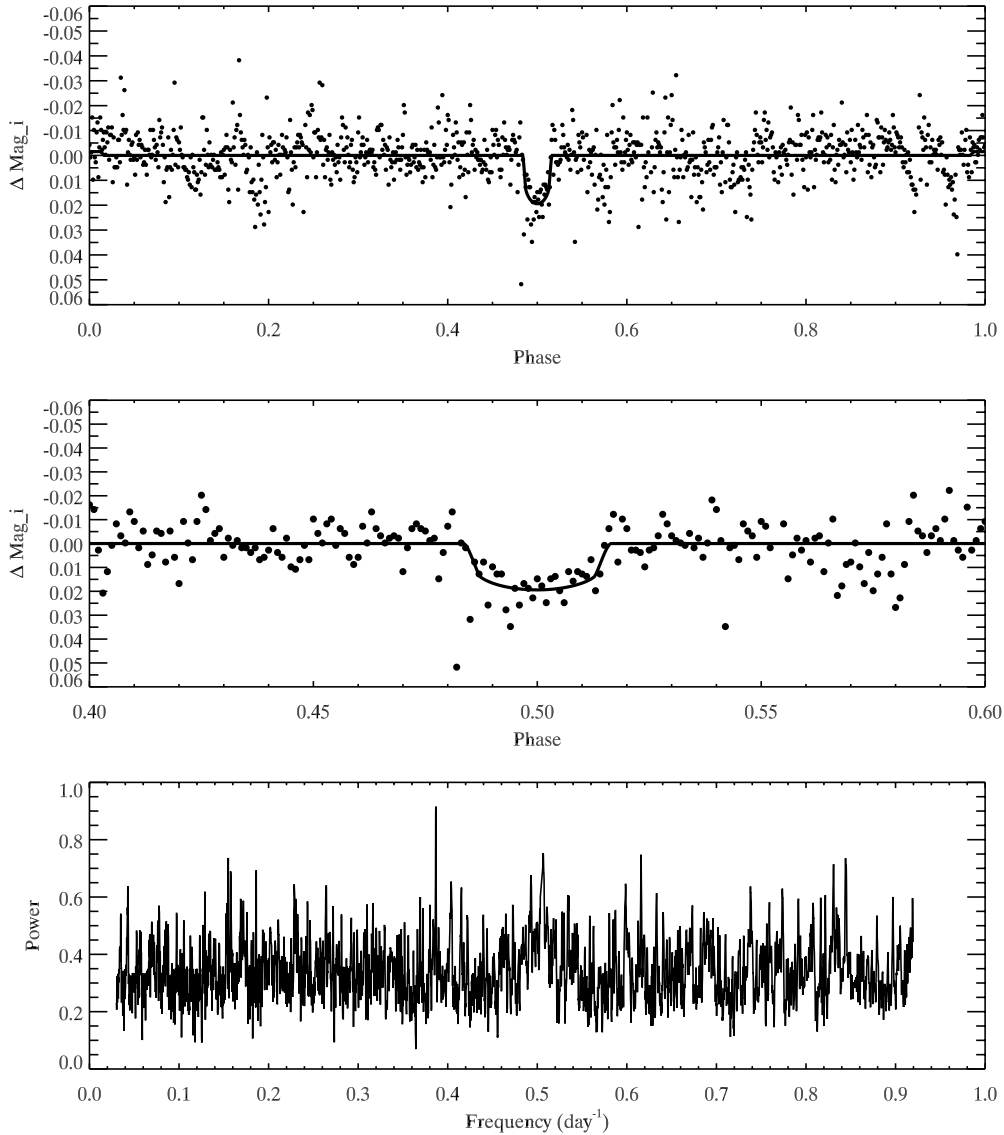


Figure 8. Same as Figure 3, but phase folded for $p = 2.586$ days for CSTAR J022810.02-871521.3 ($i = 10.62$).

4. *No statistical differences between odd and even transits.* A blended or grazing eclipsing binary system can produce a shallow dip similar to an exoplanet transit. A true exoplanet would ideally lead to evenly spaced transits with the same depths. In contrast, the depths of primary and secondary eclipses of blended or grazing eclipsing binaries are generally different due to the difference in size and temperature of the two components. In addition, the primary and secondary eclipse are usually unevenly spaced in the time series since the orbit of binaries is generally eccentric (Wu et al. 2010). We use the significant level of the consistency in transit depth (P_δ) and epoch (P_t), as detailed in Wu et al. (2010), to assess whether the odd and even transits are drawn from the same population. The smaller this statistic, the more likely the event is an astrophysical false positive. A significance level (P_δ or P_t) of 0.05 or less denotes the transit signal is unlikely to be caused by a transiting planet.
5. *No aperture blends.* Blended eclipsing binary systems are some of the most common imposters identified as

transiting planets in wide-field transit surveys such as CSTAR. The large plate-scale of CSTAR makes it likely that there will be more than one bright object within a single CSTAR pixel (15 arcsec) or the applied photometric aperture (radius = 45 arcsec) of the CSTAR photometry. This can lead to a dilution of depth of a stellar eclipsing binary, making it appear similar to a transiting exoplanet. If the angular separation of the blend is less than or comparable to the pixel scale of CSTAR, we cannot eliminate the false positive arising from blended eclipsing in this step; however, imposters arising from the wider blends can be eliminated here. The candidates are eliminated if the center of a brighter object is present within a 45 arcsec aperture.

In addition, for some candidates, aperture photometry is subject to contamination by nearby bright objects (just outside the photometric aperture). A detected transit-like shallow dip could be due to a nearby object with a deep eclipse. These spurious candidates are rejected by comparing their light curves to those of nearby objects.

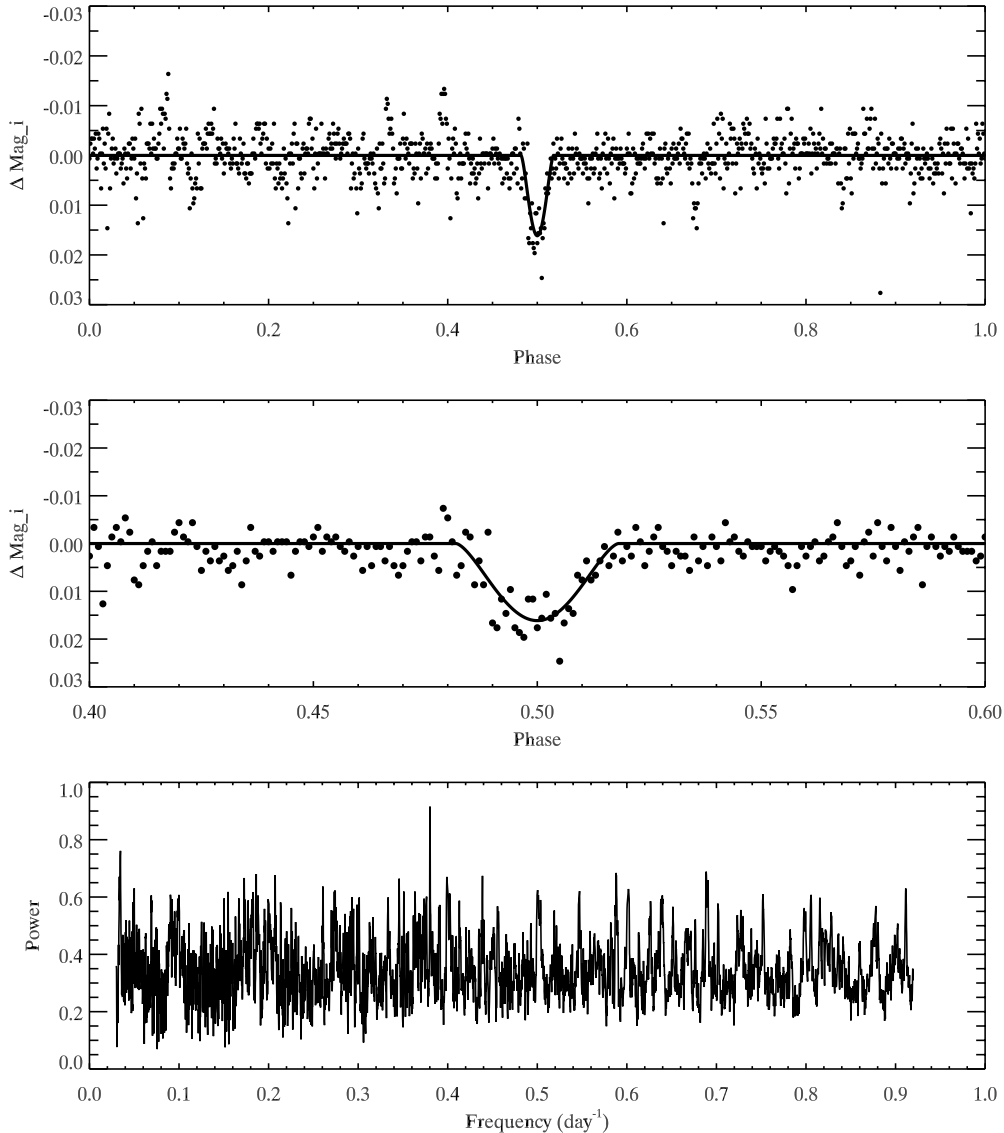


Figure 9. Same as Figure 3, but phase folded for $p = 2.630$ days for CSTAR J075108.62-871131.3 ($i = 10.41$).

We note that to avoid missing some interesting systems, some candidates with parameters just outside these thresholds have also been carried forward to the next stage. We find just 10 candidates of the initial 208 candidates pass through these statistical filters.

3.2.4. Stage 4: Additional System Information

The 10 candidates that pass through the third stage are analyzed in the following manner:

1. *Stellar information.* To estimate the radius of the transiting candidate, the radius of the host star must be determined. The color indices, derived from *Tycho-2 B-V* (Høg et al. 2000), are used to estimate the spectral type and radius of the host stars based on the data from Cox (2000), assuming the host stars to be main sequence.

Using the Besancon model (Robin et al. 2003) we estimate that 40% of the stars in our FOV between $i = 7.5$ –12 are giants, for which the detected transit signals would then be due to other stars, not planets. Taking Brown (2003) as a guide, the Two Micron All Sky Survey (2MASS) $J-K$ colors (Cutri et al. 2003) can act as a rough

indicator of the luminosity class of the target. Candidates with $J - K > 0.5$ are flagged as potential giants.

2. *Refined transit parameters.* The remaining transit light curves are modeled using the jktebop code (Southworth et al. 2004). The refined parameters of these systems, such as period, epoch, and particularly the planetary radius (R_p), are obtained from these modeling results together with the derived host stellar radius (R_*). Although gas giant planets, brown dwarfs, and white dwarfs can all have similar radii, we regard CSTAR candidates with estimated radii less than $2 R_{\text{Jup}}$ as realistic candidates.
3. *The ratio of the theoretical duration and the observed duration (η).* For each candidate, we provide the ratio of the theoretical duration and the observed duration (η), which was introduced for the OGLE candidates by Tingley & Sackett (2005) and has been successfully applied to the WASP candidates. The η of a strong exoplanet candidate is expected to be close to 1.

The analysis set out in this section was only to provide additional information to remaining systems but we did not use it to cull any candidates.

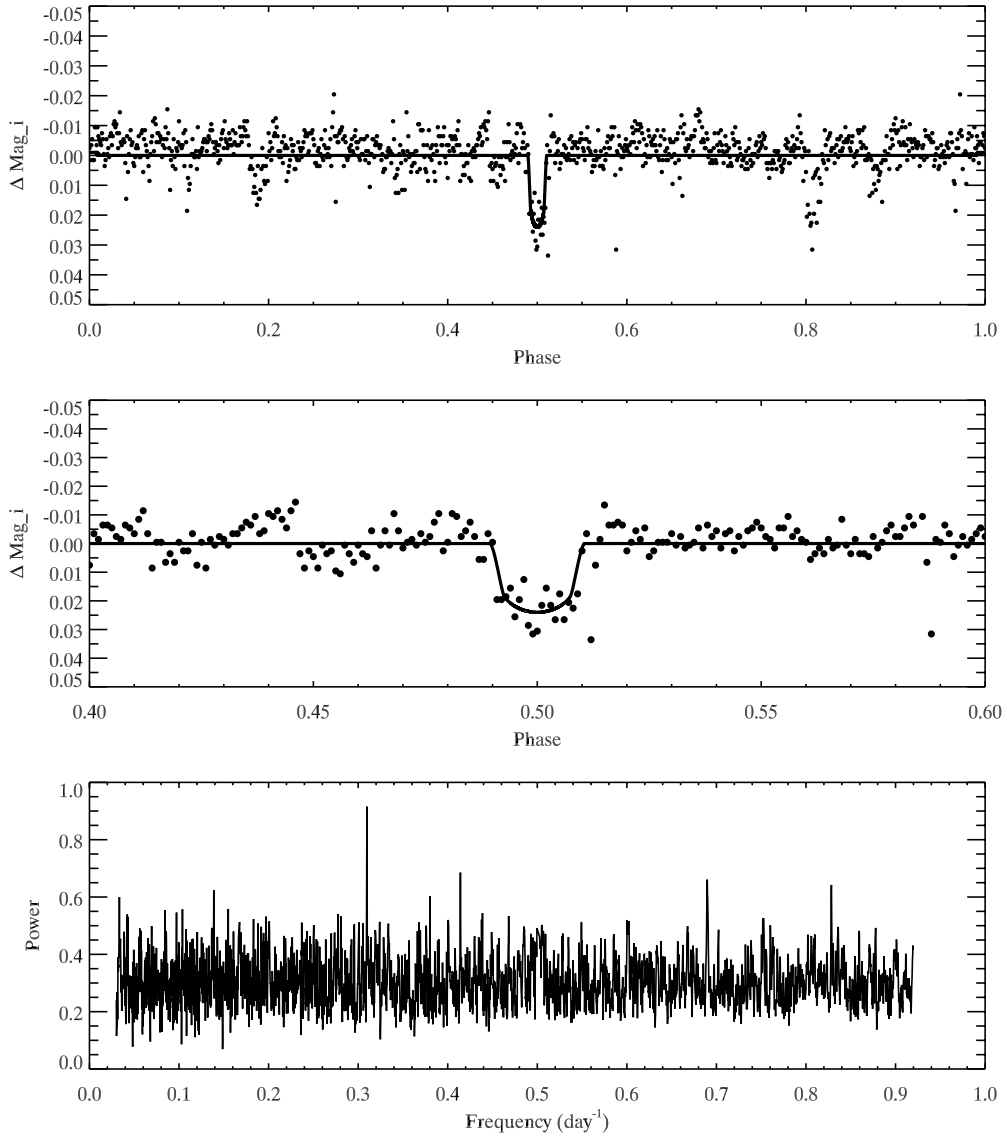


Figure 10. Same as Figure 3, but phase folded for $p = 3.228$ days for CSTAR J110005.67-871200.4 ($i = 10.84$).

4. FOLLOW-UP OBSERVATIONS

In this section we describe the follow-up spectroscopy that we have undertaken to help identify two common sources of false positives in transit surveys: eclipses around giant host stars and eclipsing binaries.

4.1. Spectral Typing Follow-up

If a candidate host star is a giant, then its large stellar radius means that the transit event seen in the discovery data cannot be due to a transiting exoplanet. We therefore spectral typed each of the 10 candidates to check for giant hosts. On the night of 2013 September 9 we took a single spectrum of each candidate with the Wide Field Spectrograph (WiFeS; Dopita et al. 2007) on the Australian National University (ANU) 2.3 m telescope. Spectra were taken using the B3000 grating which results in a resolution of $R = 3000$ and a wavelength range of 3500–6000 Å. Spectra were reduced and flux calibrated in accordance with the methodology set out in Bayliss et al. (2013). The spectra were compared to a grid of template spectra from the MARCS models (Gustafsson et al. 2008). The candidates *CSTAR J021535.71-*

871122.5, *CSTAR J014026.01-873057.1*, *CSTAR J203905.43-872328.2* and *CSTAR J231620.78-871626.8* all showed $\log g < 3.1$, indicating that they are giants and can be ruled out as candidates. The six remaining candidates are dwarfs and we therefore continued with multiple epoch RV measurements for these candidates to check for high-amplitude RV variations indicative of eclipsing binaries.

4.2. Radial Velocity Follow-up

For the six dwarf candidates, we obtained multi-epoch RV measurements using WiFeS with the R7000 grating. Details on the technique for obtaining RV measurements on WiFeS are set out in Bayliss et al. (2013). On the nights spanning 2013 September 20–25 we took between 3 and 5 RV measurements for each of six candidates spanning a range of phases for each candidate. None of the candidates showed any RV variation beyond the intrinsic measurement scatter of 2 km s^{-1} , indicating that none of these are unblended eclipsing binaries. All six therefore remain good candidates for future high-resolution RV follow-up and/or photometric follow-up.

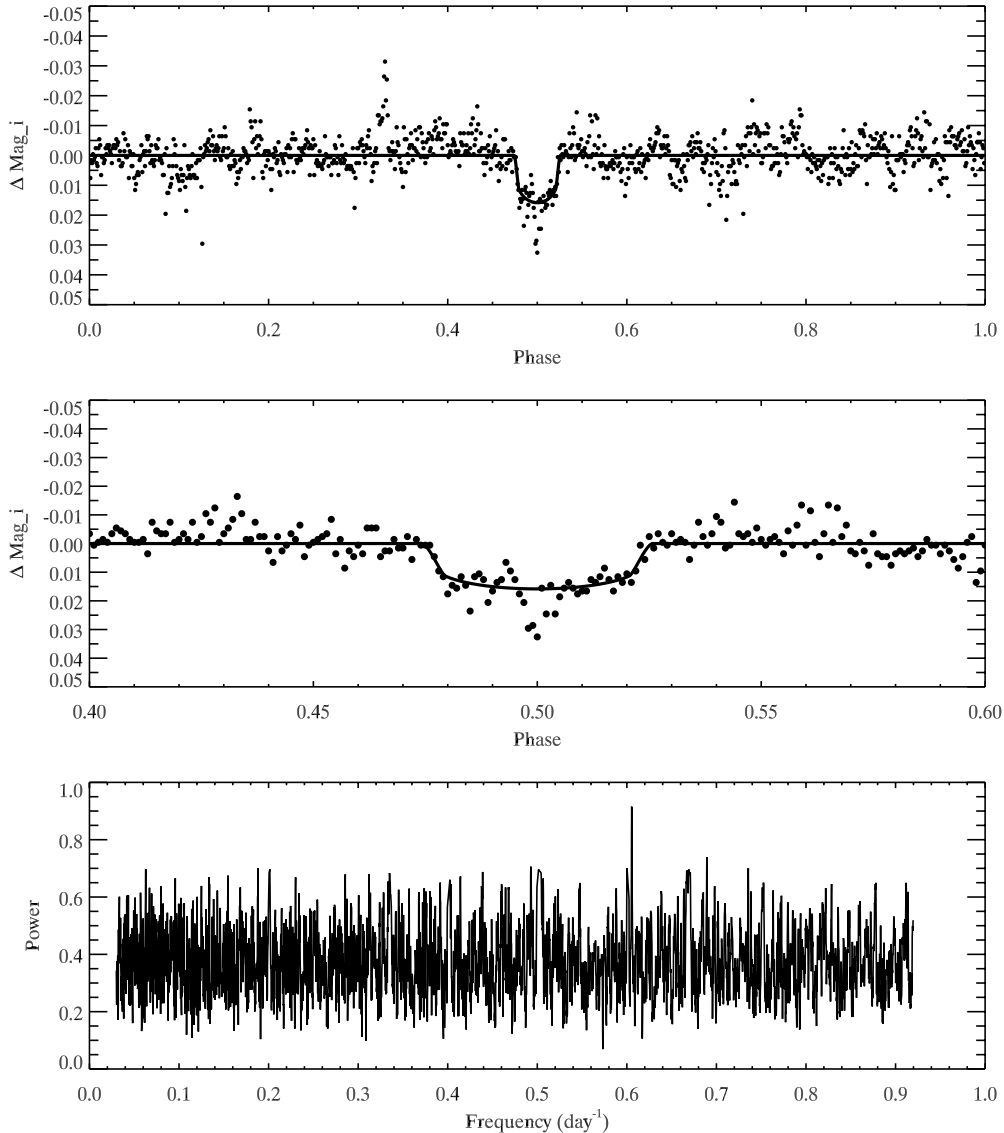


Figure 11. Same as Figure 3, but phase folded for $p = 1.652$ days for CSTAR J113310.22-865758.3 ($i = 9.97$).

5. RESULT AND DISCUSSION

In this section, we present the 10 CSTAR candidates in detail and discuss the follow-up observations we have made for each candidate.

5.1. Result of Transit Search

The candidate selection process results in 10 promising exoplanet candidates, 4 of which were found to be giants using spectroscopic follow-up. Medium-resolution RV showed none of the remaining six candidates have an RV variation greater than 2 km s^{-1} . All of these candidates are listed in Table 1, along with detailed information about them. The candidate ID is of the form “CSTAR Jhhmmss.ss – ddmms.ss,” with the position coordinates based on the *Tycho* (J2000.0) position (Høg et al. 1998).

In Figure 2, we plot the theoretical curves of the transit depth produced by planets of 0.5, 1.0, and 1.5 Jupiter radii as a function of host star radius assuming a central crossing transit ($i = 90^\circ$). All of the candidates are shown as open circles. Those with giant host stars are over-plotted as crosses. It can be seen that all

of the six remaining candidates have reasonable planetary radii between 0.5 and $1.6 R_J$.

5.2. Discussion of Candidates

In this section, we provide a detailed description of each of the 10 candidates. In addition, and for completeness, we also discuss the system “CSTAR J183056.78-884317.0,” an eclipsing binary with a light curve that is similar to a transiting exoplanet light curve and which has been previously identified by other groups. The details are summarized in Table 1. The binned phase-folded light curves of these candidates along with their respective BLS periodograms are shown in Figures 5–14.

1. *CSTAR J183056.78-884317.0*. As shown in Figure 3, this system exhibits a classic, flat-bottomed transit signature in the binned folded light curve of this bright ($i = 9.84$) star and there is a strong periodic peak at 9.93 days from 13 detected transits. However, a relatively marked ellipsoidal variation ($S/N_{\text{ellip}} = 5.87$) together with a long duration (~ 10 hr) and high value of η (2.03), suggest that it is more likely to be an eclipsing binary. This object is also identified by the ASTEP team (Crouzet et al. 2010) and another

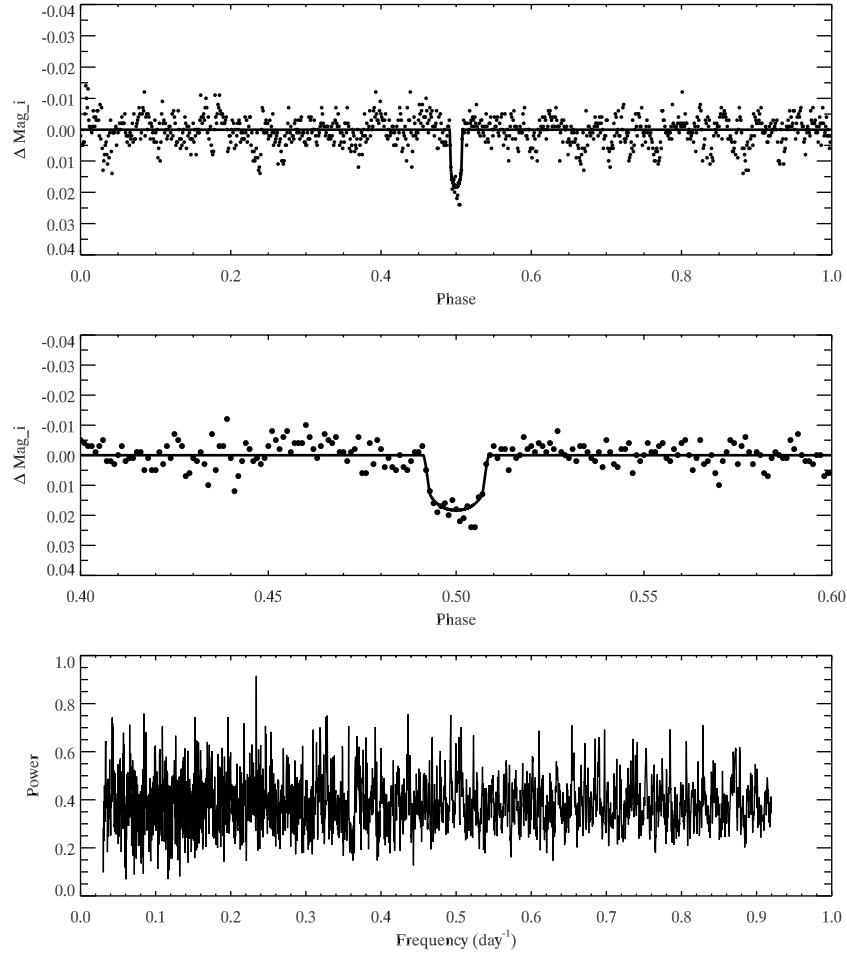


Figure 12. Same as Figure 3, but phase folded for $p = 4.273$ days for CSTAR J132821.71-870903.3 ($i = 10.41$).

CSTAR analysis team (Wang et al. 2011). To verify our analysis results, the spectroscopic observations are applied to the object using both the low-resolution WiFeS (WiFeS; Dopita et al. 2007) and the higher-resolution echelle on the ANU 2.3 m telescope. The results from five observations are presented in Figure 4 and show an RV semi-amplitude of $K = 12 \text{ km s}^{-1}$, indicating that the candidate is an eclipsing binary. The ASTEP identification of this candidate is detailed in Crouzet et al. (2013).

2. *CSTAR J001238.65-871811.0*. This candidate has 24 transits with 2% depth and has the longest period (5.37 days) of the 10 candidates. The companion radius of $0.96 R_J$ is supported by a slightly low but acceptable value of η (0.65). As all parameters of this candidate easily pass the transit-shift threshold, it is worth high-priority follow-up, although there is a relatively large scatter in the light curve and periodogram (Figure 5).
3. *CSTAR J014026.01-873057.1*. As show in Figure 6, the object displays a relatively shallow (0.9%) transit in an otherwise flat, if noisy, folded light curve with a well-defined period of 4.16 days. The *Tycho-2* color ($B - V = 1.5$) suggests an M4 primary with $0.71 R_\odot$, leading to a rather small planetary radius of $0.52 R_J$ and a reasonable $\eta = 0.71$ if it was a dwarf. However, the very red color of the host star ($J - K = 0.67$) suggested it was more likely to be a giant (Brown 2003) and this was confirmed by our spectroscopic follow-up which gave $\log(g) = 0.6$.
4. *CSTAR J021535.71-871122.5*. Although there is some scatter in the light curve over the transit (Figure 7), there is a strong peak in the periodogram. The observed short period (1.438 days) may place this candidate as a very hot Jupiter. The exceptional high $\Delta x^2 / \Delta x^2_-$ (2.69) and S_r (12.10) together with low S/N_{ellip} (0.48) plus well agreed odd and even transits make this seem a strong candidate. However, the infrared color of the host star ($J - K = 0.80$) suggests this object may be a giant and this was confirmed by our spectroscopic follow-up ($\log(g) = 3.3$).
5. *CSTAR J022810.02-871521.3*. The object displays a transit with a strong period (2.586 d) in an otherwise flat, if noisy, folded light curve (Figure 8). The F-type primary star implies a $1.55 R_{\text{Jup}}$ companion (the largest companion of the 10 candidates) and an acceptable η (0.61). These factors, together with the high $\Delta x^2 / \Delta x^2_-$ (2.63) and low S/N_{ellip} (0.65), make this target a good candidates.
6. *CSTAR J075108.62-871131.3*. This candidate displays a clear transit-like dip in the folded light curve (Figure 9) and meets all of the selection criteria well. The low S/N_{ellip} (0.75) plus the high S_r (8.6) as well as $\eta \sim 1$ make this a strong candidate. Although the very red color of the host star ($J - K = 0.95$) suggests it may have been a giant, our spectroscopic follow-up ($\log(g) = 4.5$) suggests it is more likely to be a dwarf.
7. *CSTAR J110005.67-871200.4*. As shown in Figure 10, the transit in this candidate is obvious and there is a strong

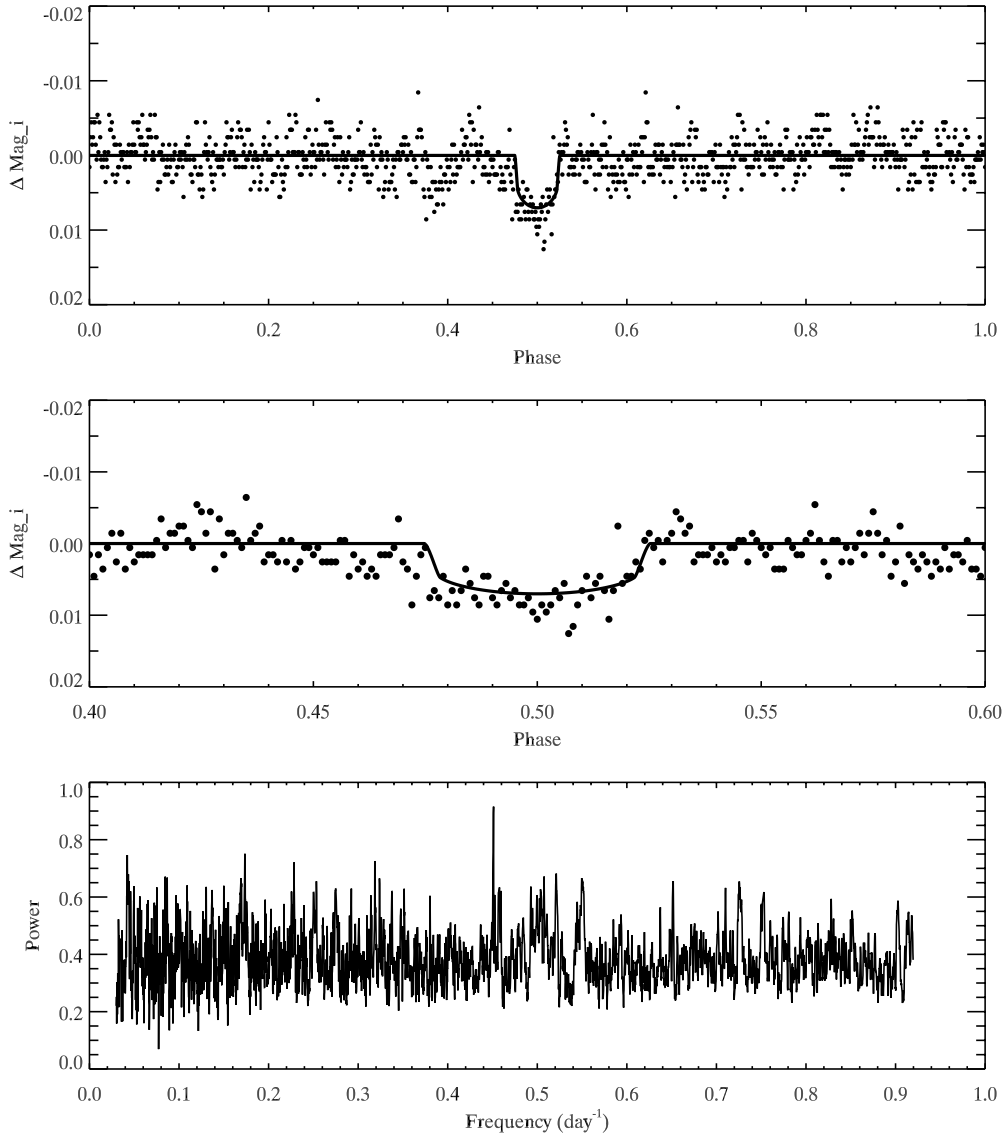


Figure 13. Same as Figure 3, but phase folded for $p = 2.216$ days for CSTAR J203905.43-872328.2 ($i = 10.35$).

peak (3.23 days) in the periodogram. The high S_r (10.6) and $\Delta x^2 / \Delta x^2$ (2.02) indicate the transit is not due to systematics. The S/N_{ellip} is low at 1.2 and the light curve is flat outside of transit. The estimate of the host radius and transit depth indicate a companion with a moderate radius ($1.34 R_{\text{Jup}}$) and an acceptable, if a bit low, η (0.55). The combination of these factors makes this candidate a high-priority target.

8. *CSTAR J113310.22-865758.3*. This candidate displays a prototypical transit of 1.5% depth over an otherwise flat, if slightly noisy, folded light curve (Figure 11). The strong peak (1.65 days) in the periodogram together with low ellipsoidal variation ($S/N_{\text{ellip}} = 2.17$) as well as a reasonable $\eta = 1.03$ indicated this brightest candidate ($i = 9.97$) is a good exoplanet candidate.
9. *CSTAR J132821.71-870903.3*. The object clearly shows a “U”-shaped dip in an otherwise flat light curve (Figure 12). This candidate has a relatively long period of 4.27 days. We derive a reasonable radius ($1.26 R_{\text{Jup}}$) of the companion for its G0 spectral type. However, an acceptable, but relatively low η (0.53) together with a slight difference between odd and even transit depth make this object a lower priority candidate.
10. *CSTAR J203905.43-872328.2*. This object displays a very shallow (~ 0.007 mag) but clear flat-bottom dip with a flat out-of-transit light curve (Figure 13) which shows no signs of ellipsoidal variation ($S/N_{\text{ellip}} = 0.53$). There is a strong peak (2.22 days) in the periodogram. The predicted relatively small companion radius of $0.64 R_{\text{Jup}}$ is slightly tempered by $\eta = 1.15$. The relatively red 2MASS $J-K$ color (0.68) suggests a possible giant host star and this was confirmed by our spectroscopic follow-up which gave $\log(g) = 1.5$.
11. *CSTAR J231620.78-871626.8*. While noisy, this folded light curve (Figure 14) exhibits a shallow transit. The strongest peak in the periodogram corresponds to 1.41 days which is the shortest companion of the final candidates. The derived radius ($0.69 R_{\text{Jup}}$) of the companion are relatively small but the calculated transit duration is close to the observed one ($\eta = 0.94$). However, the relatively red color ($J - K = 0.81$) suggested this object may be a giant and this was confirmed by our spectroscopic follow-up

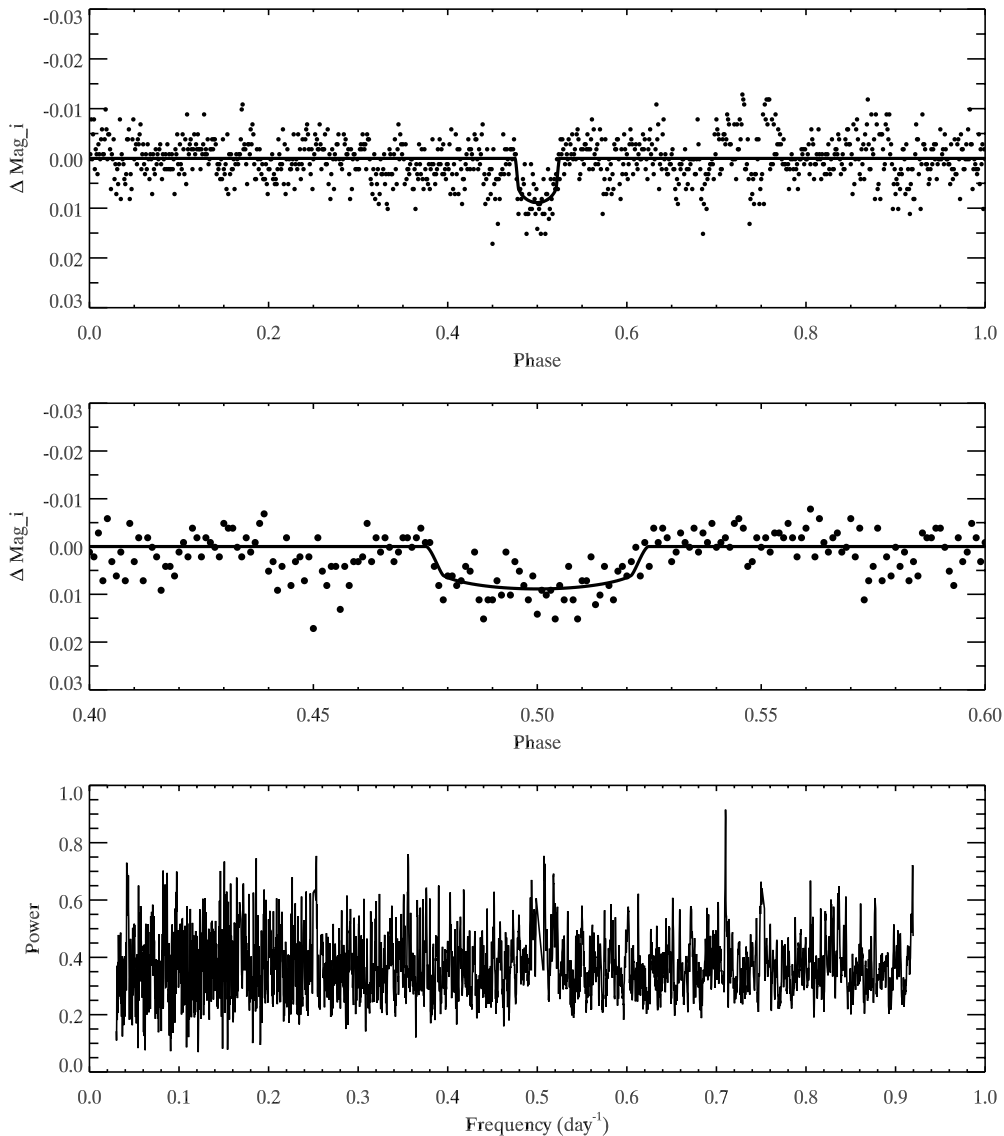


Figure 14. Same as Figure 3, but phase folded for $p = 1.408$ days for CSTAR J231620.78-871626.8 ($i = 10.76$).

($\log(g) = 1.5$). We also note that the relatively low S_r (6.7) together with a slight difference between odd- and even-transit depth indicated this candidate may have been a false positive.

5.3. Discussion of Further Follow-up Observations

The transit method has proven to be an excellent way of finding exoplanets, however, final confirmation and determination of the planetary mass and radius requires high-precision photometry and RV follow-up. Such observations of the candidates in our list are currently being performed by our colleagues in Australia.

6. CONCLUSION

In 2008, more than 100 days of observations for a 20 deg^2 field centered at the South Celestial Pole with the Antarctic CSTAR telescope provided high-precision, long-baseline light curves of 10,690 stars with a cadence of 20 s.

From this data set we found 10 bright exoplanet candidates with short periods. Subsequent spectral follow-up showed that

four of these were giants, leaving six candidates. Medium-resolution RV showed none of the six candidates have an RV variation greater than 2 km s^{-1} . These detections have enriched the relatively limited optical astronomy fruit in Antarctica and indirectly reflect the favorable quality of Dome A for continuous photometric observations.

However, the real strength of CSTAR will be realized when the 2008 data are combined with the multi-color observations of subsequent years. We expect to find many more candidates, especially those with longer periods and small radii, as a result of longer baselines along with higher signal-to-noise ratios (S/Ns).

The photometric data, including all of the CSTAR catalog and the light curves, are a valuable data set for the study of variable stars as well as hunting for transit exoplanets.

We thank the anonymous referee for suggestions that improved the manuscript. This research is supported by the National Basic Research Program of China (Nos. 2013CB834900, 2014CB845704, 2013CB834902, and 2014CB845702); the National Natural Science Foundation of China under grant Nos. 11333002, 11073032, 11003010, 10925313, 11373033,

11373035, 11203034, and 11203031; the Strategic Priority Research Program: The Emergence of Cosmological Structures of the Chinese Academy of Sciences (grant No. XDB09000000); the 985 project of Nanjing University and Superiority Discipline Construction Project of Jiangsu Province; the fund of Astronomy of the National Nature Science Foundation of China; and the Chinese Academy of Science under Grant U1231113; and the Natural Science Foundation for the Youth of Jiangsu Province (NO. BK20130547).

REFERENCES

- Alonso, R., Brown, T. M., Torres, G., et al. 2004, *ApJL*, **613**, L153
- Baglin, A., Auvergne, M., Boisnard, L., et al. 2006, in COSPAR, Plenary Meeting, 36, 36th COSPAR Scientific Assembly, ed. M. A. Shea (Amsterdam: Elsevier), 3749
- Bakos, G., Noyes, R. W., Kovács, G., et al. 2004, *PASP*, **116**, 266
- Bakos, G. Á., Csabry, Z., Penev, K., et al. 2013, *PASP*, **125**, 154
- Bayliss, D., Zhou, G., Penev, K., et al. 2013, *AJ*, **146**, 113
- Borucki, W. J., Koch, D., Basri, G., et al. 2010, *Sci*, **327**, 977
- Brown, T. M. 2003, *ApJL*, **593**, L125
- Burke, C. J., Gaudi, B. S., DePoy, D. L., & Pogge, R. W. 2006, *AJ*, **132**, 210
- Burton, M. G. 2010, *A&ARv*, **18**, 417
- Christian, D. J., Pollacco, D. L., Skillen, I., et al. 2006, *MNRAS*, **372**, 1117
- Clarkson, W. I., Enoch, B., Haswell, C. A., et al. 2007, *MNRAS*, **381**, 851
- Cox, A. 2000, *Allen's Astrophysical Quantities* (4th ed.; Berlin: Springer)
- Crouzet, N., Guillot, T., Agabi, A., et al. 2010, *A&A*, **511**, A36
- Crouzet, N., Guillot, T., Mékarnia, D., et al. 2013, in IAU Symp. 288, *Astrophysics from Antarctica*, ed. M. G. Burton, X. Cui, & N. F. H. Tothill (Cambridge: Cambridge Univ. Press), 226
- Cutri, R. M., Skrutskie, M. F., van Dyk, S., et al. 2003, *yCat*, **2246**, 0
- Daban, J.-B., Gouvet, C., Guillot, T., et al. 2010, *Proc. SPIE*, **7733**, 151
- Dopita, M., Hart, J., McGregor, P., et al. 2007, *Ap&SS*, **310**, 255
- Gustafsson, B., Edvardsson, B., Eriksson, K., et al. 2008, *A&A*, **486**, 951
- Høg, E., Fabricius, C., Makarov, V. V., et al. 2000, *A&A*, **355**, L27
- Hog, E., Kuzmin, A., Bastian, U., et al. 1998, *A&A*, **335**, L65
- Kane, S. R., Clarkson, W. I., West, R. G., et al. 2008, *MNRAS*, **384**, 1097
- Kenyon, S. L., Lawrence, J. S., Ashley, M. C. B., et al. 2006, *PASP*, **118**, 924
- Kovács, G., Zucker, S., & Mazeh, T. 2002, *A&A*, **391**, 369
- Law, N. M., Carlberg, R., Salbi, P., et al. 2013, *AJ*, **145**, 58
- Lawrence, J. S., Ashley, M. C. B., Hengst, S., et al. 2009, *RSci*, **80**, 064501
- Lister, T. A., West, R. G., Wilson, D. M., et al. 2007, *MNRAS*, **379**, 647
- McCullough, P. R., Stys, J. E., Valenti, J. A., et al. 2005, *PASP*, **117**, 783
- Meng, Z., Zhou, X., Zhang, H., et al. 2013, *PASP*, **125**, 1015
- Monet, D. G., Levine, S. E., Canzian, B., et al. 2003, *AJ*, **125**, 984
- Pollacco, D. L., Skillen, I., Collier Cameron, A., et al. 2006, *PASP*, **118**, 1407
- Pont, F., & Bouchy, F. 2005, in EAS Publications Series 14, *Dome C Astronomy and Astrophysics Meeting*, ed. M. Giard, F. Casoli, & F. Paletou (Les Ulis: EDP Science), 155
- Pont, F., Zucker, S., & Queloz, D. 2006, *MNRAS*, **373**, 231
- Robin, A. C., Reylé, C., Derrière, S., & Picaud, S. 2003, *A&A*, **409**, 523
- Saunders, W., Lawrence, J. S., Storey, J. W. V., et al. 2009, *PASP*, **121**, 976
- Sing, D. K., Désert, J.-M., Lecavelier Des Etangs, A., et al. 2009, *A&A*, **505**, 891
- Sirko, E., & Paczyński, B. 2003, *ApJ*, **592**, 1217
- Smith, A. M. S., Collier Cameron, A., Christian, D. J., et al. 2006, *MNRAS*, **373**, 1151
- Snellen, I. A. G., & Covino, E. 2007, *MNRAS*, **375**, 307
- Snellen, I. A. G., de Mooij, E. J. W., & Burrows, A. 2010, *A&A*, **513**, A76
- Southworth, J., Maxted, P. F. L., & Smalley, B. 2004, *MNRAS*, **351**, 1277
- Steinbring, E., Carlberg, R., Croll, B., et al. 2010, *PASP*, **122**, 1092
- Steinbring, E., Millar-Blanchaer, M., Ngan, W., et al. 2013, *PASP*, **125**, 866
- Steinbring, E., Ward, W., & Drummond, J. R. 2012, *PASP*, **124**, 185
- Street, R. A., Christian, D. J., Clarkson, W. I., et al. 2007, *MNRAS*, **379**, 816
- Taylor, M., Chen, K.-Y., McNeill, J. D., et al. 1988, *PASP*, **100**, 1544
- Tingley, B., & Sackett, P. D. 2005, *ApJ*, **627**, 1011
- Tosti, G., Busso, M., Nucciarelli, G., et al. 2006, *Proc. SPIE*, **6267**, 47
- Udalski, A., Paczynski, B., Zebur, K., et al. 2002, *AcA*, **52**, 1
- Wang, L., Macri, L. M., Krisciunas, K., et al. 2011, *AJ*, **142**, 155
- Wang, S., Zhou, X., Zhang, H., et al. 2012, *PASP*, **124**, 1167
- Wang, S., Zhou, X., Zhang, H., et al. 2014, *RAA*, **14**, 345
- Winn, J. N., Noyes, R. W., Holman, M. J., et al. 2005, *ApJ*, **631**, 1215
- Wu, H., Twicken, J. D., Tenenbaum, P., et al. 2010, *Proc. SPIE*, **7740**, 42
- Yang, H., Allen, G., Ashley, M. C. B., et al. 2009, *PASP*, **121**, 174
- Yuan, X., Cui, X., Liu, G., et al. 2008, *Proc. SPIE*, **7012**, 152
- Zhou, X., Fan, Z., Jiang, Z., et al. 2010a, *PASP*, **122**, 347
- Zhou, X., Wu, Z.-Y., Jiang, Z.-J., et al. 2010b, *RAA*, **10**, 279
- Zou, H., Zhou, X., Jiang, Z., et al. 2010, *AJ*, **140**, 602